POST CALIBRATION OF CHANNEL 1 OF NOAA-14 AVHRR: IMPLICATIONS ON AEROSOL OPTICAL DEPTH RETRIEVAL

Chi Li[1,4], Yong Xue[1,2], Quanhua Liu[3], Jie Guang[1], Xingwei He[1,4], Aojie Di[1,4], Lu She[1,4]*

[1] Key Laboratory of Digital Earth Science, Institute of Remote Sensing and Digital Earth, Chinese Academy of Sciences, Beijing 100094, China

[2] Faculty of Life Sciences and Computing, London Metropolitan University, 166-220 Holloway Road, London N7 8DB, UK

[3] Earth System Science Interdisciplinary Center, University of Maryland, College Park, Maryland 20740, USA

[4] University of Chinese Academy of Sciences, Beijing 100049, China

{Email: wslygr@163.com; yx9@hotmail.com}

ABSTRACT

In order to produce long-term aerosol optical depth (AOD) dataset over land from the Advanced Very High Resolution Radiometer (AVHRR), AVHRR data quality in terms of radiometric calibration must be maintained. A vicarious calibration method have been developed by incorporating well calibrated Sea-Viewing Wide Field-of-View Sensor (SeaWiFS) radiance data over several pseudo-invariant targets to inter-calibrate the channel 1 of AVHRR based on Bidirectional Reflectance Distribution Functions (BRDFs) and spectral band adjustment factor (SBAF) models for different targets. Comparison of our calibration coefficients with those of Pathfinder Atmospheres Extended (PATMOS-x) indicate the calibration accuracy to be within 2.5%. The operational L1B and recalibrated AVHRR radiance are applied to derive AOD maps over East America (dark surface) and West Africa (bright surface) using the land aerosol and bidirectional reflectance inversion by times series technique (LABITS) algorithm. Preliminary comparisons show that significant difference in the retrieved AOD from the two different calibration is expected, while the spatial distribution of AOD difference is complicated due to different surface brightness and deficiencies of numeric solutions.

Index Terms— AOD, AVHRR, radiometric calibration

1. INTRODUCTION

Long-term monitoring of global aerosols from satellite remote sensing is crucial for the climate change [1, 2] and air pollution [3] studies. The Advanced Very High Resolution Radiometer (AVHRR) is well suitable to provide continuous aerosol dataset for its successive observations of over 30 years, global coverage, moderate spatial resolution, and frequent repeat cycle [4, 5]. However, this application is significantly affected by the known calibration limitations of AVHRR data, particularly those of solar reflective channels without onboard calibration monitoring facilities [6]. Up to now there have been 16 satellites carrying AVHRR, collecting large volume of invaluable yet weakly calibrated and consequently inconsistent data. In order to overcome this obstacle for fulfilling the data application potentials, many efforts have been conducted to vicariously correct the calibration of AVHRR dataset. Meanwhile, calibration results were reported in a wide scatter (i.e. difference between results could be over 15%) as from various literatures employing a single target or method because of the difference of methods, targets, data sources, and assumptions [7]. It was anticipated that unified data sources, composite methods or targets, and well-justified approaches are essentially important for generating accurate and inter-sensor consistent AVHRR calibration.

This work aims at calibrating the channel 1 (0.63 μm) of AVHRR onboard NOAA-14 for the application of aerosol retrieval. A multi-target calibration method and a multi-observation time-series retrieval scheme have been adopted, which are addressed in Section 2. Analysis of calibration results as well as AOD retrievals are presented in Section 3. In Section 4 our work are concluded and several future works are implied.

2. METHOD

2.1. Calibration Approach

Seven pseudo-invariant targets (PTs) [8] endorsed by the the Committee on Earth Observation Satellites (CEOS) Working Group on Calibration and Validation (WGCV) are adopted for the radiometric signal characterization (Figure 1). With exclusively stability of surface characteristics and atmospheric dynamics, these targets could build a transfer path between the un-calibrated sensor and the well calibrated reference sensor. Multi-target method (including six desert targets and one Antarctic snow target in this work) are especially meaningful for reducing the systematic calibration error from a single target, increasing observation samples, expanding dynamic range, and consequently largely improving the calibration robustness [9].

To capture the actual Bidirectional Reflectivity Distribution Function (BRDF) characteristics of the PTs, we rely on the well calibrated Sea-Viewing Wide Field-of-View Sensor (SeaWiFS) radiance data with unprecedentedly high data quality and long-term stability (better than 1% to produce water-leaving radiances within 5%) [10, 11]. SeaWiFS data quality is discovered to deteriorate slightly over time according to BRDF fitting effectiveness in different periods, therefore mean SeaWiFS top of atmosphere reflectance (ρ^{TOA}) of a

* Corresponding author

3×3 window of early mission (1997-2001) channel 6 (0.67 μm) data over each PT is selected if the cloud-free and homogeneity standards are met. A BRDF model with fixed model parameters is generated to describe the ρ^{TOA} variation of different data over each PT. The Ross-Li model [12] is adopted to generate the BRDF parameters for the desert targets, and a snow BRDF model [13] was used for Dome-C. According to the preferable fitting precisions in Table 1, these BRDF parameters thus could be used to predict the SeaWiFS observed ρ^{TOA} at any observing geometry Ω for each PT within 2%, as in Eq. (1).

$$\rho^{TOA} = BRDF(\Omega) \tag{1}$$

Then the predicted TOA reflectance should be converted to that seen by AVHRR, via spectral band adjustment factor (SBAF) i.e. the ratio of TOA reflectance observed by the two sensors [14].

$$\rho_A^{TOA} = \rho_S^{TOA} \times SBAF(SRF_A, SRF_S, \Omega, r_s, ATM) \tag{2}$$

Eq. (2) means that SBAF is jointly determined by various factors including the spectral response function (SRF) of each sensor, Ω, surface reflectance r_s, and atmospheric conditions (ATM). For PTs variations of surface reflectance and aerosol scattering are minimal, and we consider the main effects from SRF, r_s and gaseous absorption (ozone absorption dominant for this band). Over 10,000 MODTRAN 4.0 simulations are conducted to calculate SBAF between AVHRR channel 1 and SeaWiFS channel 6 for two types of targets considering different observing geometries and ozone columns (oz). We build a parameterized model to predict the SBAF.

$$SBAF = \sum_{k=0}^{1} a_k(M) \times oz^k, a_k(M) = \sum_{i=0}^{4} b_i \times M^i$$
$$M = \cos(\theta_s) + \cos(\theta_v) \tag{3}$$

Where M is the geometry air mass factor representing a large part of atmospheric transfer path effects (θ_s and θ_v are the solar and view zenith angle, respectively). The model precision of our parameterization is presented in Table 2. The biases (mean errors) are very close to zero and the root mean squares (RMSs) of modelling error are within 1.5%. The time series of AVHRR digital counts (DCs) and oz values from temporally nearest ERA-Interim record for each cloud-free and homogenous AVHRR measurement over the PTs have been collected, and then the theoretically predicted AVHRR ρ^{TOA} are calculated according to Eq. (1) and (2) based on the BRDF and SBAF models. Calibration slope S for each record is derived via Eq. (4).

$$\frac{\rho^{TOA} \times \cos\theta_s}{d^2} = S(DC - ZC)/100 \tag{4}$$

Where d stands for the Earth–Sun distance factor and the zero count (ZC) is 41 according to the CLAVR-x program (ftp.ssec.wisc.edu/clavr/clavrx_satellite_constants). Every qualified AVHRR measurement over each PT results in a calibration slope. These independent estimates are combined to derive a quadratic polynomial expression as a function of time as Eq. (5), to predict calibration slope at any specific time during the lifetime of every satellite.

$$S = \sum_{i=0}^{2} C_i \times D^i \tag{5}$$

Where C_i is the fitted coefficients and D represents time expressed in days since the January 1 of 1995 as the beginning year with data availability.

2.2. Aerosol Retrieval

To demonstrate the utility of the AVHRR data in aerosol retrieval over dark and bright land surface, the recalibrated TOA reflectance were applied to retrieve AOD over East America (EA, see in Figure 3d) and West Africa (WA, see in Figure 4d), based on the land aerosol and bidirectional reflectance inversion by times series technique (LABITS) algorithm [15]. This AOD retrieval requires four continuous observations over the same area. Specifics of study areas and periods are listed in Table 3. For comparison the AODs retrieved from the operational L1B reflectance are also generated.

3. RESULTS AND ANALYSIS

3.1. Calibration Slopes

The calibration results are presented in Figure 2, where different colored points represent the measured PTs. Increasing temporal trends in the slopes are obvious, indicating the significant degradation in this channel thus calibration slopes increase to compensate for this degradation. It is notably found that the scatter points of different colors are almost distributed evenly around the fitted line for both channels of every satellite, proving that the similar yet independent calibration procedures above each PT result in consistent calibration slope (or sensor degradation) magnitudes and trends and supporting our anticipation of using multiple PTs for a robust calibration. To test whether the derived time series of calibration slopes are practical and applicable, we also plot the operational L1B and the Pathfinder Atmospheres Extended (PATMOS-x) [16] calibrations. It is found that the L1B calibration updates are not regular with obvious discontinuities, which is not in accordance to the gradual sensor degradation, whereas the magnitudes and trends of calibration slopes are more similar between this work and PATMOS-x. Quantitative comparison of the two post calibrations exhibits bias and RMS within 2.5%, strongly proving the reasonability and applicability of our derived calibration results.

3.2. AOD from Different Calibrations

As shown in Figure 2, the L1B calibration slopes are significantly lower than those from our work, indicating that the ρ^{TOA} at 0.63μm generated by our calibration would be overestimated compared to that from L1B operational calibration. This overestimation generally results obvious difference in retrieved AOD as shown in Figure 3c and Figure 4c. For EA in Figure 3, AODs are mostly overestimated as a result of our calibration (Figure 3c), in accordance to the "brightening" effects of aerosol on the TOA signal received by sensors over dark land surfaces. Meanwhile as ρ^{TOA} increases in the recalibrated AVHRR data, the AOD over WA are not entirely overestimated but exhibited a considerably underestimation for the vast desert surfaces as indicated in Figure 4d. This underestimation of AOD is mainly due to the "darkening" effects of aerosols on at sensor radiance over bright surfaces.

It should be noted that the retrieval sensitivity of ρ^{TOA} with respect to AOD is determined not only by the surface reflectance (r_s) but also by the aerosol composition and observing geometry. That is why we also discover several pixels with negative AOD difference in the EA AOD maps. This uncertainty of AOD difference distribution is further complicated by the numeric solution adopted by the LABITS algorithm, in which consecutive four-day cloud-free observations with possibly very different aerosol types and observing geometries (namely, very different retrieval sensitivities) are combined to search for an optimization (The requirement of no cloud for four observations, reducing a large part of retrievable pixels, is also a major shortcoming of LABITS). As it can be seen, the ambiguity of AOD difference is more distinctive in Figure 4c (positive and negative differences appear together) as the range of r_s are more widely

distributed in WA, where conditions with r_s very close to the critical reflectance [17] would be met and aerosol retrieval sensitivity is so week that nearly zero retrieval differences could be found.

A preliminary validation of the retrieved AOD using collocated Aerosol Robotic Network (AERONET) data has also been done. Figure 5 shows that the calibration inserts no improvement on the correlation of the satellite retrieved AOD with field truths since the algorithm is not modified, while systematic increase of the fitted slope (from 0.829 to 0.844) in the recalibration derived AOD validation imply that our calibration could provide more accurate measurement which leads to more representative satellite retrieved aerosol distribution. Overall, the AOD differences are significant as revealed by the comparison before and after post calibration in Figures 3 and 4, with difference reaching as large as 0.3, indicating very urgent need to use reliable calibration in producing AOD dataset from AVHRR.

4. CONCLUSION

A calibration method to generate channel 1 AVHRR reflectance of NOAA-14 is proposed, and the recalibrated data are applied to retrieve AOD over both dark and bright land surfaces. The multi-target calibration method is proved to be robust and reliable according to comparisons with PATMOS-x, and AOD difference as retrieved from L1B and recalibrated ρ^{TOA} are significant. We plan to use recalibration coefficients of more satellites with AVHRR onboard to support generating long-term aerosol dataset covering over 35 years for a wide range of scientific studies.

ACKNOWLEDGMENTS

This work was partly supported by the Major International Cooperation and Exchange Project of National Natural Science Foundation of China (NSFC) under Grant No. 41120114001, the NSFC (Grant No. 41271371) and the Ministry of Science and Technology, China, under Grant No. 2013CB955804. The AVHRR and SeaWiFS data are respectively from NOAA/NESDIS (http://www.class.ncdc.noaa.gov/saa/products/welcome) and the Ocean Color website (http://oceancolor.gsfc.nasa.gov). The ERA-Interim reanalysis data over the PTs are provided by the ECMWF data repository (http://data-portal.ecmwf.int/data/d/interim_full_daily/). The data for validation come from AERONET (http://aeronet.gsfc.nasa.gov/). The authors are greatly thankful to the workers in establishing and maintaining various data and processing tools used in this investigation.

REFERENCES

[1] J. M. Haywood, V. Ramaswamy, and B. J. Soden, "Tropospheric Aerosol Climate Forcing in Clear-Sky Satellite Observations over the Oceans," *Science,* vol. 283, no. 5406, pp. 1299-1303, 1999.

[2] Y. J. Kaufman, D. Tanré, and O. Boucher, "A satellite view of aerosols in the climate system," *Nature,* vol. 419, no. 6903, pp. 215-223, 2002.

[3] J. Al-Saadi, J. Szykman, R. B. Pierce *et al.*, "Improving National Air Quality Forecasts with Satellite Aerosol Observations," *Bull. Amer. Meteor. Soc.*, vol. 86, pp. 1249–1261, doi: http://dx.doi.org/10.1175/BAMS-86-9-1249, 2005.

[4] H. Akiko, and T. Nakajima, "Development of a Two-Channel Aerosol Retrieval Algorithm on a Global Scale Using NOAA AVHRR," *J. Atmos. Sci.*, vol. 56, pp. 924–941, 1999.

[5] M. I. Mishchenko, I. V. Geogdzhayev, B. Cairns *et al.*, "Aerosol retrievals over the ocean by use of channels 1 and 2 AVHRR data: sensitivity analysis and preliminary results," *Applied Optics*, vol. 38, no. 36, pp. 7325-7341, 1999.

[6] C. Cao, X. Xiong, A. Wu *et al.*, "Assessing the consistency of AVHRR and MODIS L1B reflectance for generating Fundamental Climate Data Records," *Journal of Geophysical Research*, vol. 113, doi:10.1029/2007JD009363, 2008.

[7] C. C. Molling, A. K. Heidinger, W. C. Straka *et al.*, "Calibrations for AVHRR channels 1 and 2: review and path towards consensus," *International Journal of Remote Sensing*, vol. 31, pp. 6519-6540, 2010.

[8] P. Teillet, and G. Chander, "Terrestrial reference standard sites for postlaunch sensor calibration." *Canadian Journal of Remote Sensing*, vol. 36, pp. 437-450, 2010.

[9] L. Sun, X. Hu, M. *Guo et al.*, "Multisite Calibration Tracking for FY-3A MERSI Solar Bands". *IEEE Transactions on Geoscience and Remote Sensing*, vol. 50, pp. 4929-4942, 2012.

[10] R. A. Barnes, R. E. Eplee, G. M. Schmidt *et al.*, "Calibration of SeaWiFS. I. Direct Techniques," *Applied Optics*, vol. 40, no. 36, pp. 6682-6700, 2001.

[11] R. E. Eplee, W. D. Robinson, S. W. Bailey *et al.*, "Calibration of SeaWiFS. II. Vicarious Techniques," *Applied Optics*, vol. 40, no. 36, pp. 6701-6718, 2001.

[12] C. B. Schaaf, F. Gao, A. H. Strahler *et al.*, "First operational BRDF, albedo nadir reflectance products from MODIS," *Remote sensing of Environment,* vol. 83, pp. 135-148, 2002.

[13] S. G. Warren, R. E. Brandt, and P. O. Hinton, "Effect of surface roughness on bidirectional reflectance of Antarctic snow," *Journal of Geophysical Research*, vol. 103, pp. 25789–25807, 1998.

[14] G. Chander, N. Mishra, D. L. Helder *et al.*, "Applications of spectral band adjustment factors (SBAF) for cross-calibration," *IEEE Transactions on Geoscience and Remote Sensing*, vol. 51, pp. 1267-1281, 2013.

[15] Y. Li, Y. Xue, G. de Leeuw *et al.*, "Retrieval of aerosol optical depth and surface reflectance over land from NOAA AVHRR data," *Remote Sensing of Environment*, vol. 133, pp. 1-20, 2013.

[16] A. K. Heidinger, W. C. Straka, C.C. Molling *et al.*, "Deriving an inter-sensor consistent calibration for the AVHRR solar reflectance data record," *International Journal of Remote Sensing*, vol. 31, pp. 6493-6517, 2010.

[17] F. Seidel, and C. Popp, "Critical surface albedo and its implications to aerosol remote sensing," *Atmospheric Measurement Techniques*, vol. 5, pp. 1653-1665, 2011.

Table 1. BRDF modeling performance over the PTs. Errors are presented as percent difference relative to the mean (bias stands for the mean modeling error, and RMS is the root mean square).

Site	bias (%)	RMS (%)
Algeria-3	-0.164	1.418
Algeria-5	0.085	1.450
Libya-1	-0.131	1.272
Libya-4	-0.141	1.174
Mauritania-1	-0.101	1.760
Mauritania-2	-0.860	2.042
Dome-C	0.222	2.072

Table 2. SBAF modeling performance compared to the simulated values (error terms are same as in Table 1).

Target Type	Desert	Snow
bias (%)	0.009	0.005
RMS (%)	1.428	1.572
Max Error (%)	3.180	2.887
Min Error (%)	-4.354	-4.518

Table 3 Specifics of the AOD retreival experiments.

Area	EA	WA
Domain	90°W - 70°W 25°N - 45°N	10°W - 10°E 0° - 20°N
Period	October 23 – 26, 1995	July 15 – 18, 1995

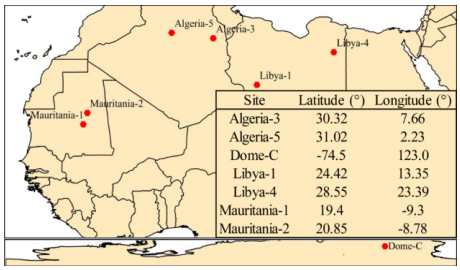

Site	Latitude (°)	Longitude (°)
Algeria-3	30.32	7.66
Algeria-5	31.02	2.23
Dome-C	-74.5	123.0
Libya-1	24.42	13.35
Libya-4	28.55	23.39
Mauritania-1	19.4	-9.3
Mauritania-2	20.85	-8.78

Figure 1. Situation of employed PTs.

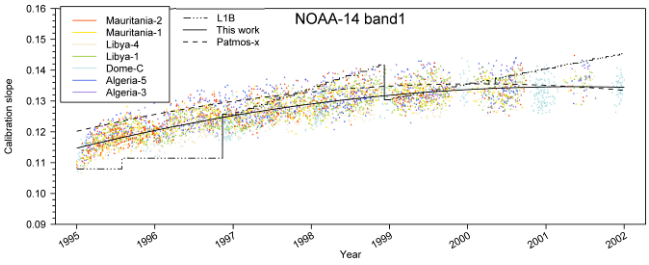

Figure 2. Time series calibration slopes of NOAA-14 channel 1. The L1B and PATMOS-x calibration slopes are also shown.

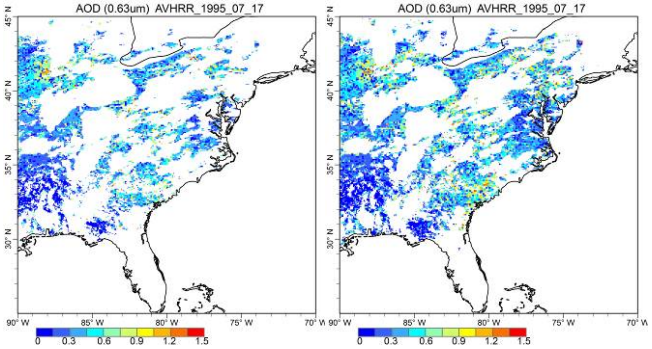

(a) (b)

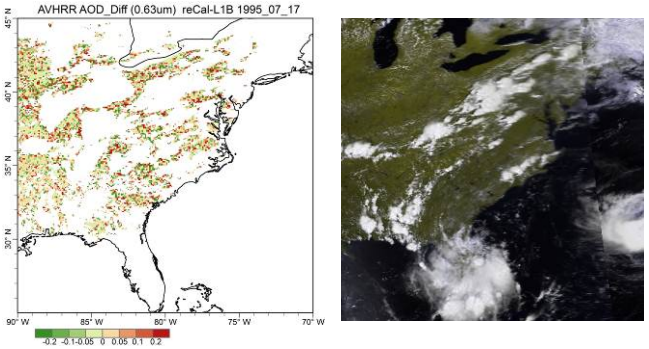

(c) (d)

Figure 3. (a) AOD retrieved from L1B calibration, (b) AOD retrieved from this post calibration, (c) AOD difference of two retrievals (this work minus L1B), and (d) False RGB image (R: band2, G: band2, B: band1) for 17th July 1995 over east America.

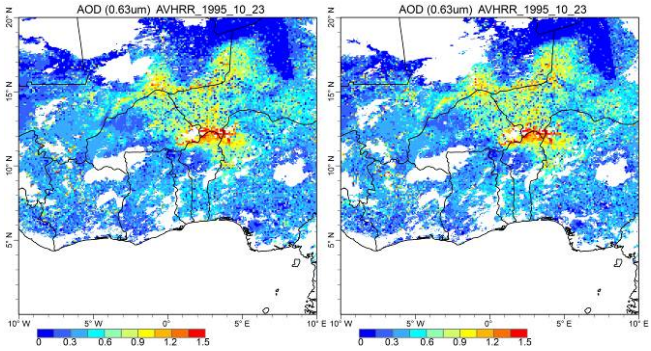

(a) (b)

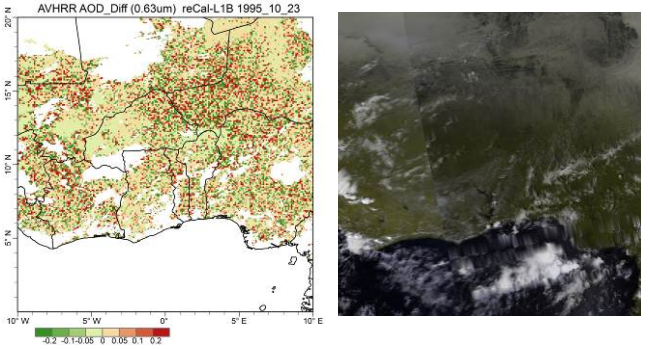

(c) (d)

Figure 4. Same as Figure 3 but for 23rd October 1995 over west Africa.

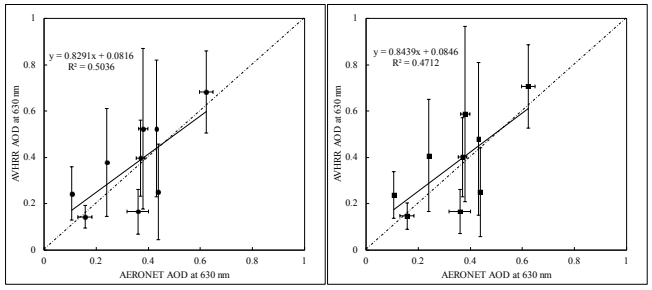

Figure 5. Validation of AOD retrieval using AERONET data (left: AOD from L1B calibration; right: AOD from this post calibration).